Evaluating robust entanglement on a trapped ion platform

Kathleen Hamilton*, Titus Morris, and Raphael Pooser
Computational Science and Engineering Division, Oak Ridge National Laboratory, Oak Ridge TN, USA
Email: *hamiltonke@ornl.gov

Kübra Yeter-Aydeniz
Emerging Technologies and Physical Sciences Department,
The MITRE Corporation, McLean, VA, 22102-7539 USA

Luning Zhao
IonQ Inc,
4505 Campus Dr, College Park, MD 20740, USA

Nouamane Laanait
Carelon Digital Platforms, Atlanta GA, USA

Harrison Cooley
Department of Physics Georgetown University,
Washington DC, USA

Muhun Kang
Department of Physics Cornell University, Ithaca NY, USA

George Barron, and Sophia Economou
Department of Physics Virginia Tech,
Blacksburg VA, USA

Akhil Francis, and Alexander Kemper
Department of Physics North Carolina State University,
Durham NC, USA

***Abstract*—We present proof of principle results for evaluating an entanglement volumetric benchmark [1] on trapped ion platforms. The benchmark quantifies the robustness of multipartite and bipartite entanglement using stabilizer measurements and witness functions. Each n-qubit graph state is prepared and used to evaluate n state-specific stabilizer strings. These stabilizer measurements are used to evaluate entanglement witness functions. The entanglement benchmark defines families of graph states associated with an initial sub-graph of the hardware qubit connectivity – with all-to-all connectivity, trapped ion systems provide a flexibility in the choice of this initial graph, and this will affect the associated family. In this work we present results targeting several classes of entangled states: 1)1-D cluster states, 2) n-qubit GHZ states, and 3) cycle graph states. These states have been found in the literature as standard hardware benchmarks, and have connections to many near-term applications.**

***Index Terms*—quantum benchmarking**

I. Introduction

Entanglement encompasses non-local correlation that provides an indication of non-classical behavior. It is a valuable resource in quantum sensing, metrology and networking [2] and there are several well-established entangled resource states of use in measurement-based computing [3]. Overall, preparing (and verifying) large-scale entangled states is a hardware benchmark that can be used on different noisy intermediate scale quantum (NISQ) platforms (superconducting qubits, trapped ions, photonics) [4]–[6].

Recently, we introduced a volumetric benchmark based on the generation of entanglement in n-qubit states [1]. Volumetric benchmarks are a hardware characterization framework that assign a score to hardware based on evaluating a fixed metric, across an ensemble of quantum states. The metric leverages specific properties of unweihgted graph states: local complementation of graphs and efficient state characterization via entanglement witnesses [7]–[9]. Local complementations are simple transformations can be applied to the graph, and the associated graph state circuit to generate a family of entangled states. Graph states are commonly utilized in many NISQ applications, for variational ansatz, they are also encountered in proofs for quantum advantage [10], and can serve as an algorithmic primitive particularly for optimization [11]. In this paper we report the performance of trapped ions on the volumetric benchmark introduced in [1].

II. Methods

A. Volumetric Benchmarking

Unweighted graph states provide us a flexible and extensible means of generating families of entangled states which also provides insight into the hardware capabilities. The benchmark is evaluated by generating multiple related graph states on

NISQ hardware, measuring the appropriate witness functions, and determining the treewidth or circuit length at which genuine entanglement cannot be verified. The results reported in [1] used superconducting qubits and a large number of randomly sampled graphs. In this section will describe the elements of the volumetric benchmark, and highlight differences in how experiments are executed on cloud-accessed trapped-ion hardware and how the metric is reported.

Volumetric benchmarking is used to define a general score for hardware based off of the evaluation of a family of circuits with varying width and secondary characteristic (commonly circuit depth). This benchmark uses graph state circuits of varying width, and the secondary characteristic is the graph state's associated treewidth. From these two quantities, we defined the robust entanglement score (RES) as a hardware characteristic defined by the graph state with maximum circuit width and treewidth that can be prepared and in which genuine entanglement can be verified. Additionally, the score is distinguished between the naïve construction and the unitary construction. The RES score associated with the naïve construction (RES-N) is the n-qubit graph with the largest treewidth that can be constructed directly from the graph's edge set. The RES score associated with the unitary construction (RES-U) is the n-qubit graph state with the largest treewidth that can be generated from another graph in the orbit.

A given NISQ device is characterized by the connectivity between qubits, the qubit design and the hardware noise. When using trapped ions, the general execution of the benchmark remains the same: the construction of graph states, and the evaluation of witness functions.

B. Graph state construction

An unweighted graph state is defined by an undirected, simple graph $\mathcal{G}(V, E)$. Given a graph $\mathcal{G}$, a graph state is prepared as follows: the vertex set $V(\mathcal{G})$ are the physical qubits in the state and the edge set $E(\mathcal{G})$ defines the set of entangling operations. The state $|\psi_{\mathcal{G}}\rangle = |i, s\rangle$ prepared on a n-qubit register initialized as $|+\rangle^{\otimes n}$ and then the set of two-qubit entangling operations are implemented by applying control-Z gates along the pairs of qubits (vertices) connected by edges, $e_{ij} \in E(\mathcal{G})$.

The graph $\mathcal{G}$ is stored as a NetworkX object. The two-qubit gates are added to the circuit by iterating over the associated edge list of the NetworkX graph object. The orientation and ordering of the two-qubit gates is defined by the ordering of the edge set. There are multiple ways of implementing controlled rotation gates on NISQ hardware, we follow the decomposition used previously in [12]: each control Z gate is decomposed into a CNOT gate and two Hadamard gates acting on the target qubit. Overall, the set of control-Z gates commute, and the unitaries are symmetric if the original graph is un-directed [13]. The ordering of the gate orientation does not affect the final graph state and the performance can be improved through optimal gate scheduling. However, in these initial proof of principle results the graph state construction is not optimized in minimizing the number of clock time steps, the gate layout does not schedule gates to reduce gate depth.

C. Entanglement Witnesses

Unweighted graph states are stabilizer states and $\mathcal{G}(V, E)$ is also used in the verification of multipartite entanglement using witness functions. For each vertex in $v_k \in V(\mathcal{G})$ there is an associated generator constructed from the Pauli Z, X operators,

$$g_k^{(\mathcal{G})} = X^{(k)} \prod_{l \to k} Z^{(l)}, \tag{1}$$

where $l \to k$ denotes the product over all neighbors of vertex (k). For vertices that are not neighbors of (k) an identity operator is inserted. Each n-qubit graph state has n generators. These Pauli strings are measured and their expectation values are used to compute the entanglement witness function. The genuine entanglement witness operator $\mathcal{W}_{\mathrm{G}}$ can be constructed using all generators:

$$\mathcal{W}_{\mathrm{G}} = (n-1)\mathbb{1} - \sum_k g_k^{\mathcal{G}}. \tag{2}$$

These measurements are done serially by preparing the graph state and measuring each individual Pauli string.

The witness function is lower bounded (ideal value) by -1, and $\mathcal{W} < 0$ indicates the presence of entanglement. For the upper bound we use the fully decohered state as a comparison point – in which case each generator $g_i \to 0$. Then the genuine witness is upper bounded by $(n-1)$.

D. LC equivalence

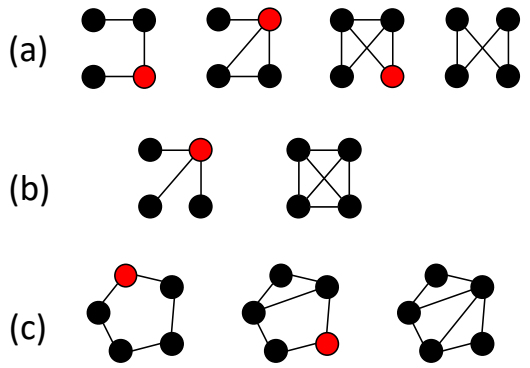

Fig. 1. Examples of how the local complement generates different graph orbits dependent on the starting graph. In each figure the local complement is defined at each step using the vertex highlighted in red. (a) Samples generated from the graph orbit of a linear cluster state $Cl(n = 4)$. (b) The exact graph orbit of the clique graph $K(n = 4)$. (c) Samples generated from the graph orbit of a cycle graph $R(n = 5)$.

Evaluating the benchmark uses samples from a finite set of graphs related to a chosen initial graph $\mathcal{G}$. This set of graphs are defined by local complement operations (LC). The LC of a graph $\mathcal{G}$ is implemented at a vertex $v_i \in V(\mathcal{G})$ and uses the edge set of the neighborhood graph $N(v_i)$. The complement of the neighborhood graph $N'(v_i)$ is used to define $\mathcal{G}' = \mathcal{G} \bigcup N'$.

An example of LC operation on different graphs is shown in Fig. (1).

The first approach to using this transformation is to redefine $\mathcal{U}_{\rm G}$. The LC operation is applied to the underlying graph, and the resulting graph $\mathcal{G}'$, is then used to construct the graph state circuit. This method of modifying the underlying graph may lead to graph state circuits with two qubit gates that do not embed onto the hardware with minimal overhead. As a result this method may incur additional noise and overhead in the form of swap gates, but the definition of the stabilizer strings $\mathcal{S}'_X$ will only use the measurement settings X, Z. However, this is not a primary concern when evaluating the benchmark on trapped ions these platforms can support all-to-all connectivity.

LC equivalent states can be implemented using local Clifford gate [13], [14]. The LC operation modifies the graph state circuit $\mathcal{U}_{\mathcal{G}} \rightarrow \mathcal{U}'_{\mathcal{G}'}$ and also modifies the stabilizer strings $\mathcal{M}_{\mathcal{S}} \rightarrow \mathcal{M}_{\rm LC(\mathcal{S})}$. Graphs related by LC transformations correspond to graph states that are in the same equivalence class defined by local unitary operations (LU). These states are different, $|\mathcal{G}\rangle \neq |\mathcal{G}'\rangle$, but both have the same degree of entanglement [13], [14]. This method of using local Clifford gates to implement LC operations keeps the number of two-qubit gates minimal but the translation of the Pauli strings may require additional measurement settings (X, Y, Z).

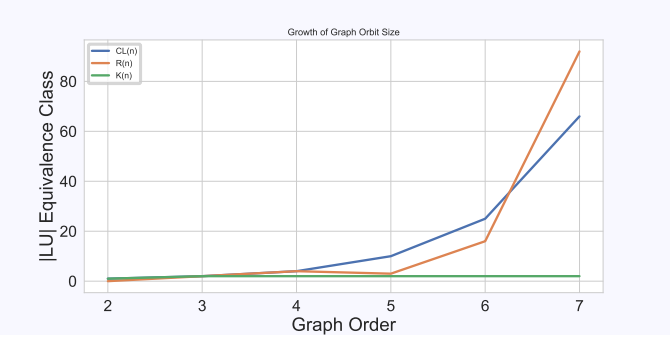

Fig. 2. Scaling of the set of LU equivalent, but not isomorphic graphs for the linear cluster state ($Cl(n)$), the cycle graph $R(n)$, and the clique graph $K(n)$.

E. Data Collection on Trapped Ions

The majority of experiments were conducted on the trapped ion platform *Harmony*. The data was collected intermittently from May 2021 through July 2022. The Harmony platform consists of 13 $^{171}\mathrm{Yb}^{+}$ ions which are aligned to form a linear crystal with spacing of about 4μm and suspended in a chip trap with a radial pseudo-potential frequency of $\approx$ 3.1MHz. It offers all-to-all connectivity between 11-qubits [15], [16]. 11 out of 13 total qubits are utilized as computational qubits and the two end ions were used to provide a more uniform spacing of the central 11 ions. A second set of experiments were executed on the *Aria* platform in August 2022. The Aria platform offers all-to-all connectivity between 23-qubits. For both platforms IonQ reports an average single-qubit, two-qubit fidelities, and SPAM errors since the calibration is conducted constantly. The Aria system has much higher single- and two-qubit gate fidelities compared with the Harmony system.

The data collection on the trapped ion platform was can be summarized as follows. The experiments were conducted using $n = 3 - -7$, qubits. Each circuit was sample using $N_{\rm shots} = 1024$shots on Harmony and $N_{\rm shots} = 8192$ shots on Aria.

The different initial graph states that were used: a $n-$qubit linear cluster state (a $Cl(4)$ qubit example is shown in Fig. 1), or a $n-$qubit cycle graph state, a n-qubit star graph, or the $n-$qubit clique (a $n = 4$ qubit example is demonstrated in Fig. 3). Circuit batching was not used to gather data therefore, each experiment is conducted independently.

The `Qiskit-IonQ` Provider was used to access the IonQ platforms. This provider provides the opportunity to use IBM's `Qiskit` programming language construct circuits that will be deployed on IonQ's hardware. The state preparation circuit is constructed in `Qiskit` then translated into instructions for execution on IonQ hardware through the `qiskit-ionq` plugin which implements IonQ's transpilation and compilation pipeline.

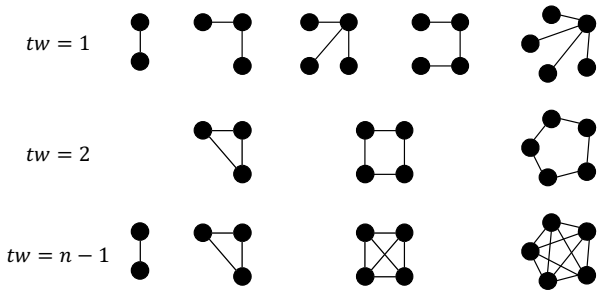

Fig. 3. Examples of graphs with $n \leq 5$ vertices and their treewidths. Tree graphs have $tw = 1$, cycle graphs have $tw = 2$, cliques have $tw = (n-1)$. Enumeration of graph examples is not exhaustive.

The single-qubit gates used in IonQ hardware are GPI gate, GPI2 gate and GZ gate which are defined as

$$GPI(\phi) = \begin{pmatrix} 0 & e^{-i\phi} \\ e^{i\phi} & 0 \end{pmatrix},$$

$$GPI2(\phi) = \frac{1}{\sqrt{2}} \begin{pmatrix} 1 & -ie^{-i\phi} \\ -ie^{i\phi} & 1 \end{pmatrix},$$

$$GZ(\theta) = \begin{pmatrix} e^{-i\theta/2} & 0 \\ 0 & e^{i\theta/2} \end{pmatrix}.$$

The two-qubit entangling gate used on trapped ion platforms is the Mølmer-Sørenson gate which is defined as

$$MS = \frac{1}{\sqrt{2}} \begin{pmatrix} 1 & 0 & 0 & -i \\ 0 & 1 & -i & 0 \\ 0 & -i & 1 & 0 \\ -i & 0 & 0 & 1 \end{pmatrix}. \quad (3)$$

The transpilation into IonQ basis gate sets is optimized to use the smallest set of laser pulses and the experiment

TABLE I

MINIMUM GENUINE WITNESS FOR CL(N) AND R(N) INITIAL STATE EVALUATED ON HARMONY. CL(N) DATA COLLECTED MAY 2021 AND OCTOBER 2021, R(N) DATA COLLECTED MAY 2021.

Genuine (Cl(n)), $n < 7$				
N	3	4	5	6
tw	1	1	1	1
$\mathcal{W}_G$	-0.804	-0.767	-0.564	-0.484

Genuine (R(n)), $n < 7$				
N	3	$--$	5	6
tw	2	$--$	2	2
$\mathcal{W}_G$	-0.818		-0.558	-0.28

is execute onto the ideal ions and gates as determined by up-to-the minute calibrations. Because of this optimization process readout error correction was not implemented in the experiments.

III. RESULTS

We separate the results according to the different intial states used: linear cluster state $Cl(n)$, cycle graphs $R(n)$, and GHZ states (i.e. the clique graph) $K(n)$. We report the minimum value of the genuine witness functions for each graph in the following table. From Figs. 1 and 3 we highlight that with 3 qubits, the graph orbit of $(Cl(n))$, $(K(n))$ and $(R(n))$ are the same, there are only 2 unique graphs.

A. $Cl(n)$ and $R(n)$ States

In this section we present results for the linear cluster state (Cl(n), $tw = 1$) and for the n-qubit cycle graph state (R(n), $tw = 2$). While the 4-qubit cycle appears in the orbit of Cl(n=4), the orientation of the vertices are twisted and only the explicit constructions of the n-qubit cycle graph states with $n = 5, 6$ were tested. As shown in Fig. 2 the size of the graph orbit (number of LU equivalent, but non-isomorphic graphs) grows quickly with the graph order. Additionally, as graph orbits do not intersect or share graphs, we know that the largest treewidth found in the linear cluster state orbit cannot exceed $tw = (n-2)$. Using the $Cl(n)$ state will test graphs with minimal treewidth (the initial $Cl(n)$ state), and graphs of possible treewidths up to $tw = (n-2)$.

B. GHZ States

In this section we present two sets of results for the GHZ state orbit. The first set of results were evaluated on the Harmony device using cloud-based queue access. The second set of results were evaluated on the Aria device using dedicated access. We first report the genuine witness values for preparing individual graph states. Then we present results on the genuine witness values under the effect of LU transformations. The transformations modify the graph state, and also translate the stabilizer strings.

As shown in Fig. 1 the graph orbit of the clique graph consists of the clique graph and a star graph – the GHZ state maps onto the star graph representation. As shown in Fig. 3, the star graph has $(tw = 1)$ and the clique graph has $tw = (n-1)$. Thus using the GHZ state will test the extreme limits

TABLE II

GENUINE WITNESS FOR INITIAL STATES IN THE GHZ GRAPH ORBIT EVALUATED ON HARMONY. DATA COLLECTED AUGUST 2021.

Genuine (K(n)), $n < 7$				
N	3	4	5	6
tw	2	3	4	5
$\mathcal{W}_G$	-0.818	-0.330	2.000	1.309
N	3	4	5	6
tw	1	1	1	1
$\mathcal{W}_G$	-0.804	-0.592	2.361	1.543

	Genuine (K(n)), $n = 7$	Genuine (S_k), $n = 7$
N	7	7
tw	6	1
$\mathcal{W}_G$	2.147	-0.463

TABLE III

GENUINE WITNESS FOR INITIAL STATES IN THE GHZ GRAPH ORBIT EVALUATED ON ARIA. DATA COLLECTED AUGUST 2022.

Genuine (K(n)), $n < 7$				
N	3	4	5	6
tw	2	3	4	5
$\mathcal{W}_G$	-0.838	-0.755	-0.718	0.222

Genuine (S_k), $n < 7$				
N	3	4	5	6
tw	1	1	1	1
$\mathcal{W}_G$	-0.824	-0.748	-0.747	-0.679

	Genuine (K(n)), $n = 7$	Genuine (S_k), $n = 7$
N	7	7
tw	6	1
$\mathcal{W}_G$	1.140	-0.567

of possible treewidths. We also note that in both graphs of the clique graph orbit, there is always at least one vertex with maximum degree of $n-1$.

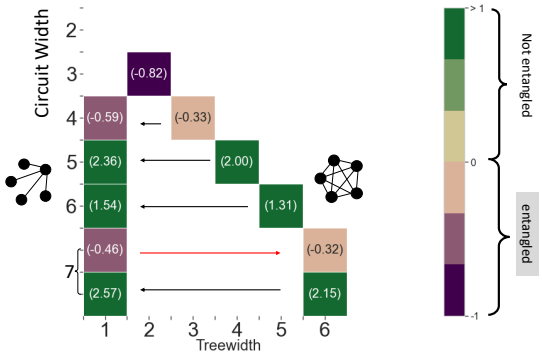

Fig. 4. Minimum multi-partite entanglement witness values using the GHZ state orbit and LU transformations on the Harmony device. The horizontal arrows indicate which state is initially prepared, then transformed through LU operations.

IV. ANALYSIS AND DISCUSSION

Robust Entanglement Score

From the GHZ state orbit results in Section III-B we can compute for Harmony the RES-N score is 12 (see Table II) since 4 qubits entangled using the full edge set of the 4-qubit clique. The RES-U score is 42 (see Fig. 4), applying LC operations to the 7 qubit S_k graph can transform it into

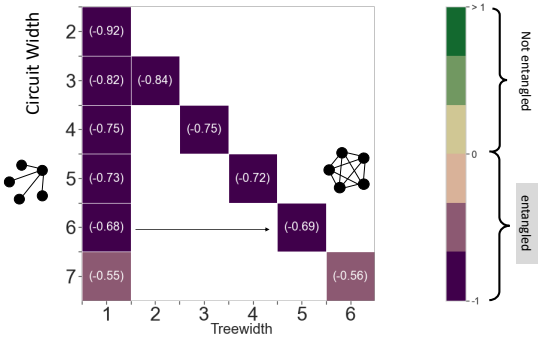

Fig. 5. Minimum multi-partite entanglement witness values using the GHZ state orbit on the Aria device. Each state is initially prepared in the S_k state then local unitaries are applied to transform into the K(n) state.

the LU equivalent complete graph state. When the initial state is S_k it is possible to generate multi-partite entanglement on all circuit widths tested. When the initial state is a clique, we were not able to prepare and verify multipartite entanglement on $n = 7$ qubits.

From the GHZ state orbit results in Section III-B we can compute for Aria the RES-N score is 20 (see Table III) since 5 qubits entangled using the full edge set of the 5-qubit clique. The RES-U score is 42 (see Fig. 5), applying LC operations to the 7 qubit S_k graph can transform it into the LU equivalent complete graph state. When the initial state is S_k it is possible to generate multi-partite entanglement on all circuit widths tested. When the initial state is a clique, we were not able to prepare and verify multipartite entanglement on $n = 7$ qubits.

The GHZ state orbit covers graphs with the maximum and minimum treewidth on n-qubits: star graphs ($tw = 1$) and clique graphs ($tw = n-1$). To test if n-qubits can be genuinely entangled on treewidth ($1 < tw < n - 1$) graphs requires a different LU class.

These classes can include the $Cl(n)$, and $R(n)$ graph. These orbits cover graphs of $1 \leq tw \leq (n-2)$. But as shown in Fig. 2, these orbits grow rapidly with graph order. In [1], the graph orbit of $Cl(n)$ graphs was sampled from using random LC sequences. This approach is not guaranteed to generate graphs that give a representative sample of all treewidth values in the orbit. The initial demonstrations reported in Section III-A only use the $Cl(n)$ or $R(n)$ initial states.

Related Work: Efforts to measure genuine multi-partite entanglement are of critical interest to studying quantum devices; it can serve as a proxy to measure the performance of the device on applications that make extensive use of entanglement. Entanglement witnesses were also recently used in a fault-tolerant weight-4 parity check measurement scheme [17]. The witnesses showed that the quantum error correction encoding circuit generates genuine six-qubit multi-partite entanglement in their shuttling-based trapped-ion quantum computer.

This work only considered graph states, which greatly simplified the construction of the entanglement witnesses. There are a number of approaches to entanglement witness construction, which are applicable to other classes of entangled states [18]–[26]. Other studies have used GHZ states as a low-level coherent noise characterization tool [27]. While this technique provides low-level information about the device and entanglement, the information gained about the device is specific to the noise model considered.

Other characterization techniques utilize graph states [28], [29] to focus on detecting entanglement in specific states rather than noise characterization. Similarly, graph state verification was recently achieved on an 18-qubit device [30]. Prior work has also inferred the entanglement present in the prepared graph state in all possible subsystems [31], but is challenging to implement for larger systems, except in special cases.

V. Conclusions

We have presented results based on verifying genuine entanglement in n-qubit graph states with varying treewidth. The use of stabilizer-based witness functions maximizes the number of qubits we can test, the overhead of the benchmark scales linearly. Through the local complementation of graph states, this benchmark can systematically test a range of entangled states.

Future work will strengthen the connection between benchmark and application performance. However, there is one near-term example in the field of quantum advantage using cyclic cluster states [32], [33] that has immediate connections to the benchmark. Furthermore, in the data collection stage there is a need for efficient sampling methods to effectively explore all possible treewidth graphs in the orbit. Finally there are many avenues for circuit design optimization such as parallelization of two-qubit gates, consolidation of one-qubit gates, or use of noise robust gate designs.

Acknowledgements

The scientific design, data collection, manuscript writing and data analysis was supported in part as part of the ASCR Testbed Pathfinder Program at Oak Ridge National Laboratory under FWP ERKJ332 (K.E.H., T. M., K.Y.A., A.F., and R. C. P.). The software development and testing (H. C. and M. K.) was supported in part by the U.S. Department of Energy, Office of Science, Office of Workforce Development for Teachers and Scientists (WDTS) under the Science Undergraduate Laboratory Internship program. A.F. and A.F.K were supported by the National Science Foundation under Grant No. NSF DMR-1752713 (for planning, formal development, and software development) and by the ASCR Testbed Pathfinder Program (data interpretation and manuscript writing). K.Y.A. was supported by MITRE Corporation TechHire and Quantum Horizon programs during data collection and manuscript writing.

References

[1] Kathleen E Hamilton, Nouamane Laanait, Akhil Francis, Sophia E Economou, George S Barron, Kübra Yeter-Aydeniz, Titus Morris, Harrison Cooley, Muhun Kang, Alexander F Kemper, et al. An entanglement-based volumetric benchmark for near-term quantum hardware. *arXiv preprint arXiv:2209.00678*, 2022.

[2] Xueshi Guo, Casper R Breum, Johannes Borregaard, Shuro Izumi, Mikkel V Larsen, Tobias Gehring, Matthias Christandl, Jonas S Neergaard-Nielsen, and Ulrik L Andersen. Distributed quantum sensing in a continuous-variable entangled network. *Nature Physics*, 16(3):281–284, 2020.

[3] Tzu-Chieh Wei. Measurement-based quantum computation. *arXiv preprint arXiv:2109.10111*, 2021.

[4] Otfried Gühne, Chao-Yang Lu, Wei-Bo Gao, and Jian-Wei Pan. Toolbox for entanglement detection and fidelity estimation. *Physical Review A*, 76(3):030305, September 2007. arXiv: 0706.2432.

[5] Tom Mainiero. Homological Tools for the Quantum Mechanic. *arXiv:1901.02011 [hep-th, physics:quant-ph]*, January 2019. arXiv: 1901.02011.

[6] Gary J. Mooney, Gregory A. L. White, Charles D. Hill, and Lloyd C. L. Hollenberg. Generation and verification of 27-qubit Greenberger-Horne-Zeilinger states in a superconducting quantum computer. *arXiv:2101.08946 [quant-ph]*, February 2021. arXiv: 2101.08946.

[7] Mohamed Bourennane, Manfred Eibl, Christian Kurtsiefer, Sascha Gaertner, Harald Weinfurter, Otfried Gühne, Philipp Hyllus, Dagmar Bruß, Maciej Lewenstein, and Anna Sanpera. Experimental detection of multipartite entanglement using witness operators. *Phys. Rev. Lett.*, 92:087902, Feb 2004.

[8] Bastian Jungnitsch, Tobias Moroder, and Otfried Gühne. Entanglement Witnesses for Graph States: General Theory and Examples. *Physical Review A*, 84(3):032310, September 2011. arXiv: 1106.1114.

[9] Bastian Jungnitsch, Tobias Moroder, and Otfried Gühne. Taming multiparticle entanglement. *Phys. Rev. Lett.*, 106:190502, May 2011.

[10] Yingyue Zhu, Austin Daniel, Cinthia Huerta Alderete, Vikas Buchemmavari, Alaina Green, Nhung Nguyen, Tyler Thurtell, Andrew Zhao, Norbert Linke, and Akimasa Miyake. Provable quantum advantage in bell-type nonlocal games with the cyclic cluster state. In *APS Division of Atomic, Molecular and Optical Physics Meeting Abstracts*, volume 2022, pages Q07–003, 2022.

[11] Maxime Dupont, Nicolas Didier, Mark J. Hodson, Joel E. Moore, and Matthew J. Reagor. An entanglement perspective on the quantum approximate optimization algorithm, June 2022. arXiv:2206.07024 [quant-ph].

[12] Yuanhao Wang, Ying Li, Zhang-qi Yin, and Bei Zeng. 16-qubit ibm universal quantum computer can be fully entangled. *npj Quantum information*, 4(1):1–6, 2018.

[13] M. Hein, W. Dür, J. Eisert, R. Raussendorf, M. Van den Nest, and H.-J. Briegel. Entanglement in Graph States and its Applications. *arXiv:quant-ph/0602096*, February 2006. arXiv: quant-ph/0602096.

[14] Adán Cabello, Lars Eirik Danielsen, Antonio J. López-Tarrida, and José R. Portillo. Optimal preparation of graph states. *Phys. Rev. A*, 83:042314, Apr 2011.

[15] Kenneth Wright, Kristin M Beck, Sea Debnath, JM Amini, Y Nam, N Grzesiak, J-S Chen, NC Pisenti, M Chmielewski, C Collins, et al. Benchmarking an 11-qubit quantum computer. *Nature communications*, 10(1):1–6, 2019.

[16] Yukio Kawashima, Erika Lloyd, Marc P Coons, Yunseong Nam, Shunji Matsuura, Alejandro J Garza, Sonika Johri, Lee Huntington, Valentin Senicourt, Andrii O Maksymov, et al. Optimizing electronic structure simulations on a trapped-ion quantum computer using problem decomposition. *arXiv preprint arXiv:2102.07045*, 2021.

[17] Janine Hilder, Daniel Pijn, Oleksiy Onishchenko, Alexander Stahl, Maximilian Orth, Björn Lekitsch, Andrea Rodriguez-Blanco, Markus Müller, Ferdinand Schmidt-Kaler, and Ulrich Poschinger. Fault-tolerant parity readout on a shuttling-based trapped-ion quantum computer. *arXiv preprint arXiv:2107.06368*, 2021.

[18] Dariusz Chruściński and Gniewomir Sarbicki. Entanglement witnesses: construction, analysis and classification. *Journal of Physics A: Mathematical and Theoretical*, 47(48):483001, December 2014. arXiv: 1402.2413.

[19] Philipp Hauke, Markus Heyl, Luca Tagliacozzo, and Peter Zoller. Measuring multipartite entanglement through dynamic susceptibilities. *Nature Physics*, 12(8):778–782, August 2016.

[20] Kyung Hoon Han and Seung-Hyeok Kye. Construction of multi-qubit optimal genuine entanglement witnesses. *Journal of Physics A: Mathematical and Theoretical*, 49(17):175303, April 2016. arXiv: 1510.03620.

[21] Farid Shahandeh, Martin Ringbauer, Juan C. Loredo, and Timothy C. Ralph. Ultrafine entanglement witnessing. *Phys. Rev. Lett.*, 118:110502, Mar 2017.

[22] Mordecai Waegell and Justin Dressel. Benchmarks of nonclassicality for qubit arrays. *npj Quantum Information*, 5(1):66, August 2019.

[23] David Amaro and Markus Müller. Design and experimental performance of local entanglement witness operators. *Phys. Rev. A*, 101(1):012317, January 2020. Publisher: American Physical Society.

[24] Bas Dirkse, Matteo Pompili, Ronald Hanson, Michael Walter, and Stephanie Wehner. Witnessing entanglement in experiments with correlated noise. *Quantum Science and Technology*, 5(3):035007, June 2020. Publisher: IOP Publishing.

[25] Jan Roik, Karol Bartkiewicz, Antonín ıfmmode \checkC\else Č\fiernoch, and Karel Lemr. Accuracy of Entanglement Detection via Artificial Neural Networks and Human-Designed Entanglement Witnesses. *Phys. Rev. Applied*, 15(5):054006, May 2021. Publisher: American Physical Society.

[26] Andrea Rodriguez-Blanco, Alejandro Bermudez, Markus Müller, and Farid Shahandeh. Efficient and Robust Certification of Genuine Multipartite Entanglement in Noisy Quantum Error Correction Circuits. *PRX Quantum*, 2(2), April 2021.

[27] You Zhou. Entanglement detection under coherent noise: Greenberger-Horne-Zeilinger-like states. *Physical Review A*, 101(1):012301, January 2020. Publisher: American Physical Society.

[28] Thomas Nutz, Antony Milne, Pete Shadbolt, and Terry Rudolph. Efficient detection of useful long-range entanglement in imperfect cluster states. *APL Photonics*, 2(6):066103, June 2017. arXiv: 1702.01958.

[29] Kh P. Gnatenko and V. M. Tkachuk. Entanglement of graph states of spin system with Ising interaction and its quantifying on IBM's quantum computer. *Physics Letters A*, 396:127248, April 2021. arXiv: 2012.05986.

[30] Ken X. Wei, Isaac Lauer, Srikanth Srinivasan, Neereja Sundaresan, Douglas T. McClure, David Toyli, David C. McKay, Jay M. Gambetta, and Sarah Sheldon. Verifying multipartite entangled Greenberger-Horne-Zeilinger states via multiple quantum coherences. *Physical Review A*, 101(3), March 2020.

[31] You Zhou, Qi Zhao, Xiao Yuan, and Xiongfeng Ma. Detecting multipartite entanglement structure with minimal resources. *npj Quantum Information*, 5(1):83, October 2019.

[32] Meron Sheffer, Daniel Azses, and Emanuele G Dalla Torre. Playing quantum nonlocal games with six noisy qubits on the cloud. *Advanced Quantum Technologies*, 5(3):2100081, 2022.

[33] A. K. Daniel, Y. Zhu, C. H. Alderete, V. Buchemmavari, A. M. Green, N. H. Nguyen, T. G. Thurtell, A. Zhao, N. M. Linke, and A. Miyake. Quantum computational advantage attested by nonlocal games with the cyclic cluster state. *Phys. Rev. Res.*, 4:033068, Jul 2022.